Journal of
Nanoscience and Nanotechnology
Vol. 11, 4852–4862, 2011

Analysis of Assembling ZnO Nanoparticles Into Nanogap Electrodes for Nanoscale Electronic Device Applications

Young-Kyo Seo[1], Sanjeev Kumar[2], and Gil-Ho Kim[1,*]

[1] *Department of Electronic and Electrical Engineering, and Sungkyunkwan University Advanced Institute of Nanotechnology, Sungkyunkwan University, Suwon 440-746, Republic of Korea*
[2] *London Centre for Nanotechnology, University College London, 17-19 Gordon Street, WC1H 0AH, London, UK*

We report the assembly of semiconducting ZnO nanoparticles into nanogap electrodes using ac dielectrophoresis (DEP) process. ZnO nanoparticles were grown using sol–gel method. As grown ZnO nanoparticles (diameter ~4 nm) were in a quasi-crystalline state and with increase in annealing temperature (in air) upto 400 °C the crystallinity was found to increase as revealed by X-ray diffraction and transmission electron microscopy. Absorption spectroscopy revealed that absorption edge of the as grown and annealed samples exhibited a blue-shift and could be attributed to the size quantization. A strong band tailing in the absorption spectra indicates the presence of shallow defects in the nanoparticles. The annealed ZnO nanoparticles (diameter ~9 nm) were assembled into nanogap electrodes (60 nm) using DEP process. DEP parameters such as frequency, applied voltage, and time were optimized to assemble ZnO nanoparticles into nanogap electrodes. Frequency variation study revealed that positive DEP is active at frequencies less than 500 kHz, and the negative DEP starts dominating at 1 MHz. It was observed that when DEP force overcomes the Brownian motion, the nanoparticles start chaining together in the region between the electrodes tip due to particle-field and particle–particle interactions. Under the optimized DEP parameters such as frequency of 150 kHz, peak-to-peak voltage of 3 V, and trapping time of 30 s, a minimum number of ZnO nanoparticles were assembled into nanogap electrodes. The ZnO nanoparticles based device was studied for field effect transistor (FET) characteristics and the typical current–voltage (I_D–V_{DS}) characteristic curves as a function of gate voltage (V_G) were obtained. The curves indicate that ZnO nanoparticles based FET exhibits a significant gate effect as the conductance of the ZnO nanoparticles increases with gate voltage suggesting *n*-type semiconducting behavior of ZnO nanoparticles. Results show the myriad potential of dielectrophoretically assembled ZnO nanoparticles into nanogap electrodes for designing nanoscale devices for electronic and optoelectronic applications.

Keywords: Nanoparticles, II–VI Semiconductors, Dielectrophoreis, Nanoscale Materials Structure: Fabrication and Characterization.

RESEARCH ARTICLE

1. INTRODUCTION

In recent years worldwide research on the assembly of ZnO nanostructure materials is gaining considerable attention. The assembly of nanostructures is one of the most important issues regarding the design and fabrication of devices for nano- and molecular electronics. The manipulation and trapping of ZnO nanostructure materials in electrodes gap could allow us to investigate the characteristics of materials at nano-scale level which can provide some intriguing properties different from those observable in their bulk counterpart. The nanostructure materials can be assembled in a wide variety of electrodes gap ranging from few micron to hundreds of nanometer. One of the most widely used methods is so-called "pick and place" method,[1] where ZnO nanostructures are dispersed randomly onto the device substrate with pre-fabricated electrodes. Using this method, individual ZnO nanostructure based devices have been developed.[2–6] However, such random dispersal method is unsuitable for controlled and reproducible manufacturing of devices. Another method which is more robust involves dispersal of ZnO nanostructures onto substrate and then selectively fabricating metal contacts on the ends of nanostructure by using lithography and lift-off techniques.[7] By using this method, ZnO nanowires and nanorods with micro-sized length have been successfully characterized,

*Author to whom correspondence should be addressed.

 1533-4880/2011/11/4852/011 doi:10.1166/jnn.2011.4140

and the fabricated devices have shown great potential for applications ranging from ultraviolet (UV) sensor,[8] field effect transistor (FET),[6, 7, 9] and chemical sensor.[10] However, this method has some drawbacks such as complicated and slow processing, and the selective deposition method is not well suited to high throughput fabrication. The two methods mentioned above have difficulty in applying to manipulation of nano-sized materials particularly nanoparticles. To accurately control and manipulate nanostructure materials in electrodes gap, a number of assembling methods have been developed such as dielectrophoresis (DEP), optical-assisted alignment, and fluidic and magnetic alignment [Ref. [11], and Reference therein]. Out of these different methods, the assembly of nanostructures using DEP method has gained a considerable attention due to its simplicity, high efficiency and high yield of the end product. Besides such miniaturized devices have many advantages such as decreased size, less power consumption, faster speed, greater sensitivities, and potentially lower fabrication cost.[12]

DEP is an electrical process where a non-uniform electrical field is applied on particles suspended in a medium. Due to the presence of non-uniform field, the particles suspended in the dielectric medium get polarized and a translational force, called as DEP force, acts whose strength and type depend on the medium and particles properties. Such DEP force can be used to manipulate particles of any kind between patterned electrodes. DEP is considered very useful in applications such as separation and sorting, purification, assembling of metallic, biological, and semiconducting materials, and various other environmental applications.[13–16]

Assembling of wideband gap semiconducting ZnO nanomaterials in electrodes gap using DEP method promises a great future for realizing devices for micro- and nanoelectronics. ZnO is a well known wideband gap (~3.3 eV) material exhibiting excellent optical and electrical properties,[17–20] and finds applications in optoelectronics such as UV lasers and detectors.[19] Recently, nanostructures of ZnO have attracted much more attention for fundamental studies as well as applications in nanodevices. Various ZnO nanostructures including nanotube,[20] nanowire,[21] nanorod[7] and other interesting nanostructures[22, 23] have been synthesized and characterized due to their great potential over bulk or film structure for next-generation nanoelectronics and optoelectronics devices. Suehiro et al.[24] demonstrated the dielectrophoretic assembly of ZnO nanowires (diameter ~100 nm, length ~2–5 μm) on microelectrodes gaps. Lee et al.[25] reported the dielectrophoretic assembly of ZnO nanowires (diameter ~120–150 nm, length ~10–15 μm) on patterned opposite pairs of electrodes with a gap of 4 μm, and characterized the FET performance on the ZnO nanowires. Also, single ZnO nanowire based Schottky diode has been fabricated by dielectrophretically aligning the synthesized ZnO nanowires onto paired electrodes.[26, 27] Irrespective of some reports on the dielectrophoretic alignment of ZnO nanostructures such as nanowires and nanorods in micron size electrodes gap,[24, 25, 28] assembling of ZnO nanoparticles in nanogap electrodes is not well documented yet.

In the present work, we report the growth and characterization of ZnO nanoparticles and their optimized assembly into nanogap electrodes using ac DEP process. DEP parameters such as applied frequency, voltage, and time have been optimized to assemble ZnO nanoparticles in 60 nm gap electrodes to create ZnO based nanodevice. The fabricated semiconductor nanodevice based on ZnO nanoparticles is electrically characterized and its potential as an FET device has been reported.

2. EXPERIMENTAL DETAILS

The Au nanogap electrodes used in the present work were fabricated on oxide-coated silicon substrate using standard electron-beam lithography and lift-off technique.[13] One chip consisted of 10 pairs of electrodes with gap size of 60 nm each. ZnO nanoparticles were grown by a simple chemical route of sol–gel process.[29] Zinc acetate dehydrate [$(Zn(CH_3COO)_2 \cdot 2H_2O)$: 1.10 gm dissolved in ethanol (70 ml)] was mixed with lithium hydroxide [$(LiOH \cdot H_2O)$: 0.29 gm dissolved in ethanol (50 ml)] under vigorous stirring. The final solution was kept at 4 °C for two days and resulted in the formation of ZnO-sol. N-heptane was slowly added to the ZnO-sol in the volume ratio of 1:2, and the final volume was again stored at 4 °C for three hour. Adding *n*-heptane led to the precipitation and ZnO-gel settled down at the bottom of the beaker. The precipitated powder was isolated, washed, and dried at room temperature. The solution containing the ZnO-gel was then heated at 150 °C for one hour to remove ethanol and the final product left was ZnO nanoparticulate powder. The ZnO nanoparticulate powder was then annealed at different temperatures from 100 to 400 °C for three hour each. The synthesized ZnO nanoparticles were characterized by using UV/VIS spectroscopy (Model: Cary 5000), X-ray diffraction (XRD) (Bruker AXS, Model: D8 FOCUS), high resolution transmission electron microscopy (HRTEM), and energy dispersive X-ray spectroscopy (EDS). After growth, the annealed ZnO nanoparticles were dispersed in dionised (DI) water and sonicated for DEP experiments. The experimental setup used for DEP assembly consists of a function generator and an oscilloscope.[30] Prior to dielectrophoretic assembly, the chip was passed through a cleaning process such as O_2 plasma cleaning and rinsing in ethanol. A drop of ZnO nanoparticles suspended in DI water was placed in the center of chip using a micropipette and immediately ac voltage was applied across the electrodes to initiate the DEP process. After DEP processing, scanning electron microscopy (SEM) (Jeol, Model: JSM-7401F) was used to examine the dielectrophoretic alignment of nanoparticles into nanogap electrodes. Field effect

transistor characteristics of the fabricated device were investigated by using *I–V* measurement system (Keithley; Model: 4200-FCS).

3. RESULTS AND DISCUSSION

3.1. Characterization of ZnO Nanoparticles

3.1.1. X-Ray Diffraction

ZnO nanoparticles grown by sol–gel method were characterized by XRD. Figure 1(a) shows the XRD spectra obtained on four samples of ZnO nanoparticles i.e., as-grown, annealed at 200, 300, and 400 °C, respectively. The diffraction peaks have been indexed as hexagonal phase of wurtzite ZnO with lattice parameters in accordance with the values in standard card (JPCDS 36-1451). With increase in annealing temperature the peaks became more sharp and intense; however, change in peak position was observed to be minimal.[31–33] The average crystallite size of the powder samples is determined by Scherer's formula

$$D = k\lambda/\beta\cos\theta \quad (1)$$

where D is the average crystallite size, K is the shape factor (taken as 0.9), λ is the X-ray wavelength (0.15 nm), β is the full width at half maximum intensity (FWHM), and θ is the diffraction angle.[33] Since ZnO nanoparticles exhibited polycrystalline behavior, nanoparticle size was estimated along different orientations. The average size of the as-grown and annealed nanoparticles (200, 300, and 400 °C) along (100), (002), and (101) planes were estimated to be 3.87, 6.38, 9.28, 9.30 nm, respectively. It may be noted that as-grown nanoparticulate powder exhibited very low intensity of peaks, and the peaks were not completely resolved in accordance with the ASTM data card of ZnO. It appears that as-grown ZnO nanoparticles were poor in crystallinity as evident by weak reflections from different planes of ZnO. An annealing temperature of 200 °C significantly affected the peak intensity, and peaks corresponding to wurtzite ZnO started appearing more clearly than as-grown samples, and the particle size increased to ~6.38 nm. A further increase in annealing temperature to 300 °C made the diffraction peaks more sharp and intense as well as the particle size increased to ~9.28 nm. Particle size was insignificantly influenced with a further increase in annealing temperature to 400 °C, however impurity diffraction peaks detected under lower annealing temperatures were significantly reduced. No characteristic peaks corresponding to any noticeable impurities (such as Li^+ and Zn^{2+}) were observed for samples annealed at 400 °C revealed the formation of crystalline ZnO nanoparticles.[34, 35] It may be noted that with an increase in annealing temperature even though crystallinity and the sharpening of diffraction peaks were found to increase significantly, however, increase in particle size was not significant unlike some reports where it is found to increase invariably with temperature.[31, 32] It may be noted that similar observations have been made by other groups. Noack and Eychmüller[33] observed that the size of ZnO remains unaffected till a temperature of 100 °C (6 nm), however, at higher temperatures (between 300 to 500 °C) the increase in particle size (50 nm) was significant. A similar trend of results was reported by Hoyer et al.[36] where an insignificant change in particle size of ZnO nanoparticles with increasing annealing temperature till 500 °C was observed. The insignificant change in the size of nanoparticles may be attributed to destabilizing nature of Li^+ during thermal treatment.[36] Even though XRD didn't show any peak corresponding to lithium, its presence cannot be ruled out due to high solubility of lithium acetate in aqueous solvents. This further indicates that Li^+ is not incorporated deep inside the ZnO lattice but could be located in first few monolayers next to the surface of the particles. Additionally, no separate crystalline lithium compounds were found in the XRD patterns for

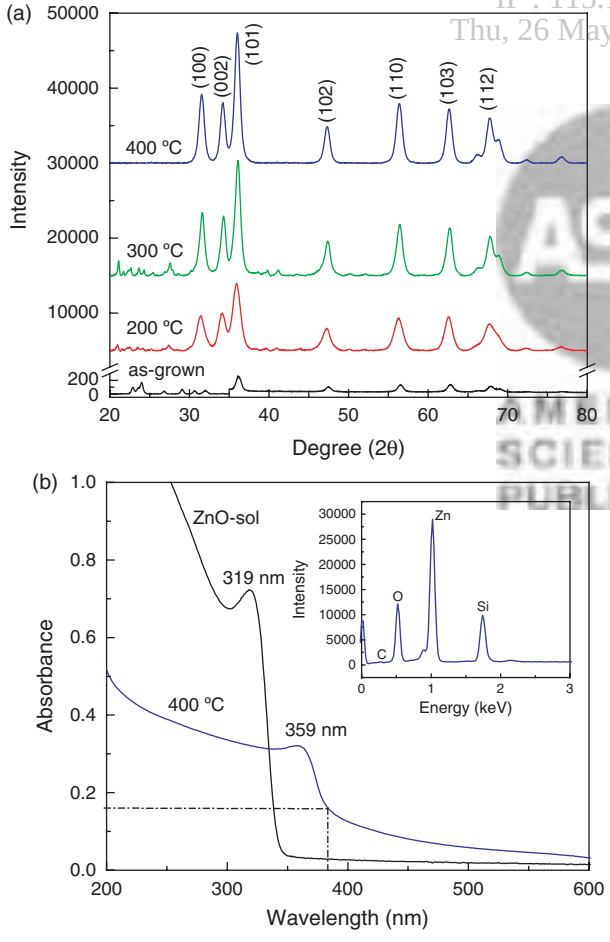

Fig. 1. (a) XRD spectra obtained on four samples of ZnO nanoparticles i.e., as-grown, annealed at 200, 300, and 400 °C, respectively; (b) The absorption spectra of ZnO-sol and 400 °C annealed ZnO nanoparticles (suspended in DI water) exhibiting the absorption peaks at 319 nm and 359 nm, respectively. Inset shows the EDS spectrum of ZnO nanoparticles annealed at 400 °C.

all samples thus ruling out a phase separation during the annealing process.[33, 36] To examine the ZnO nanoparticles growth, EDS spectrum of ZnO nanoparticles (annealed at 400 °C) was taken which shows peaks corresponding to zinc and oxygen, thus confirming the formation of ZnO (Fig. 1(b), inset). The Si peak is emanating from the silicon substrate used during the EDS measurement.

3.1.2. Absorption Spectroscopy

UV-visible spectroscopy was used to record the absorption spectrum of ZnO nanoparticles suspended in DI water at room temperature (Fig. 1(b)). The absorption spectrum corresponding to ZnO-sol is also included for comparison. It may be noted that ZnO-sol exhibited absorption peak at ~319 nm, which is blue-shifted in comparison to the absorption edge of the reference bulk ZnO which is close to 380 nm.[36] Interestingly, 400 °C annealed ZnO nanoparticles also exhibited a blue-shift in the absorption edge at 360 nm. This can be understood in terms of increase in band gap due to size quantization effect. In principle, ZnO nanoparticles exhibit a blue shift when the size of the nanoparticles is of the order of Bohr radius (~1.8 nm) and is attributed to the quantum confinement effect.[37–40] However, in the present case the nanoparticles size is more than the Bohr radius. According to previously published results, a size quantization is observed in ZnO nano-colloids when particle size is of the order of 7 nm, beyond which it is very unlikely to observe such effects.[29, 33, 41] The observation of size quantization in the present work for particle size ~9 nm might be explained on the basis that the real volume accessible is smaller than the actual geometric size of the crystallites.[33] This is evident from the XRD spectra which show the grown ZnO nanoparticles are consisting of crystallites of different orientations which in turn favor the volume than the actual geometric size. Moreover, the additional spatial confinement might arise from the presence of potential barrier at the surface which extends to the inner part of ZnO nanoparticles.[33] This potential barrier could arise due to distortion in conduction and valence band at the grain boundaries of the irregularly stacked nanoparticles. The negatively charged acetate ions present on the surface of sol–gel grown ZnO nanoparticles might electrostatically repel the inner electrons in ZnO. Additionally due to the electrostatic interactions of the acetate ions a slight band bending might occur at the surface of ZnO which could result a situation where the electronic levels inside the ZnO nanoparticles are more favored than at the surface. This could result in an increase in local electron density and shift of the lower electronic transitions towards higher energies.[33, 42–44] All these combined efforts may be attributed to the blue-shift in absorption spectra. Noack and Eychmüller[33] observed a similar behavior in the absorption spectra of nanosized ZnO thin films.

Alternatively if we consider the absorption edge corresponding to ZnO-sol as reference then with increase in annealing temperature a red-shift in the absorption spectra is observed which could be attributed to other effects either related to crystallinity of the grown material or defects present in the crystal lattice. The amorphous material is a disordered system without long range translational periodicity. Due to the amorphous nature of the material, the extended localization in the conduction and valence bands increases and a blue shift in absorption edge is observed.[39] With increase in annealing temperature the crystallinity starts building up in the amorphous ZnO, and system becomes less disorder and localization in conduction and valence bands reduces which in turn causes a red shift in the absorption spectrum (Fig. 1(b)). Similar observations have been reported in thin films of ZnO when annealed at different temperatures and blue/red shift was observed depending on growth and annealing temperature.[39] The observed red shift with annealing temperature might also be attributed to formation of shallow traps inside the band gap due to the impurity or defects states present in the crystal lattice. This also has been suggested that red-shift normally overlaps with a strong band tailing, which may disturb the local symmetry in ZnO crystal lattice.[40] With increase in temperature the band tailing is expected to reduce due to anneal out of the defects. However, presence of band tailing observed in the present work for samples annealed at 400 °C shows that defects have not been annealed out and could be responsible for the observed red-shift in the absorption edge.

3.1.3. Transmission Electron Microscopy Analysis

ZnO nanoparticles were investigated for structural and crystallographic orientation using HRTEM and selected areas electron diffraction (SAED). Figure 2 shows the SAED and HRTEM images of the as-grown and 400 °C annealed ZnO nanoparticles. As grown ZnO were appearing like crystalline ZnO nanoparticles in the matrix of amorphous ZnO. Figure 2(a) shows the SAED patterns of as-grown ZnO nanoparticles. We can see that diffraction patterns are not intense and in the center a hollow diffuse pattern indicates the possibility of amorphous ZnO. In the SAED pattern there is a broad ring which results from the contributions of both the quasicrystalline and amorphous phases. It may be noted that diffraction rings corresponding to wurtzite ZnO along (100), (101), and (110) planes show the presence of crystalline ZnO nanoparticles. In additional, some hazy diffraction rings corresponding to (112) and (200) planes are also visible. Other diffraction spots may come from nanocrystalline and approximant phases. Figure 2(b) is the bright field TEM image of the as-grown ZnO nanoparticles. It may be observed that amorphous phase in addition to crystalline phases, as indicated by fringe patterns (circled area), are visible. The inset of Figure 2(b) shows a less magnified TEM view of the as-grown nanoparticles. The TEM result is

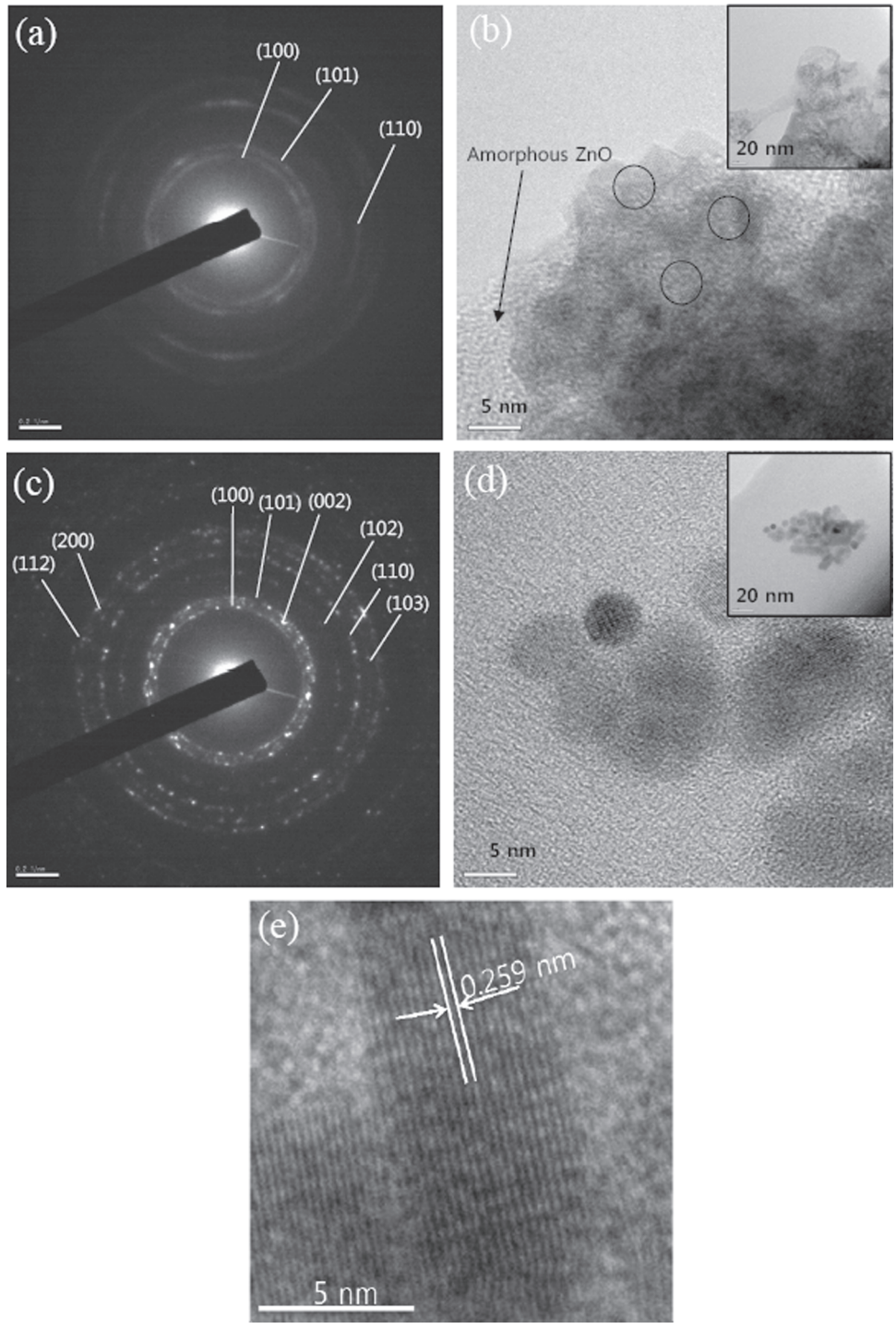

Fig. 2. TEM images of as grown and 400 °C annealed ZnO nanoparticles. (a) SAED patterns of as grown ZnO nanoparticles showing less intense diffraction patterns. In the SAED pattern there is a broad ring which results from the contributions of both the quasicrystalline and amorphous phases. It may be noted that diffraction rings corresponding to wurtzite ZnO along (100), (101) and (110) planes in addition to some diffraction patterns corresponding to (112) and (200) planes indicate the presence of crystalline ZnO nanoparticles; (b) Bright field TEM image of the as grown ZnO nanoparticles showing the amorphous phase in addition to crystalline phase, as indicated by fringe patterns (circled area). The inset shows a less magnified TEM view of the as grown nanoparticles; (c) SAED patterns obtained on 400 °C annealed ZnO samples. It may be noted that diffraction patterns are more intense and match very well to the Miller indices of wurtzite hexagonal bulk ZnO along (100), (002), (101), (102), (110), (103), (200), and (112) planes; (d) Bright field TEM image of ZnO nanoparticles annealed at 400 °C. It may be noted that randomly oriented nanoparticles with clear diffraction fringes are visible indicating crystalline quality of the annealed samples. Inset shows the nanoparticles size was varying in the range of 6 to 9 nm; (e) An HRTEM image of a single ZnO nanoparticle shows the fringes corresponding to (002) plane with a lattice spacing (d) of about 0.259 nm.

consistent with the X-ray diffraction analysis. Figure 2(c) shows the SAED patterns obtained on 400 °C annealed ZnO samples. It may be noted that diffraction patterns are more intense and match very well to the Miller indices of wurtzite hexagonal bulk ZnO along (100), (002), (101), (102), (110), (103), (200), and (112) planes. However, it was noticed that diffraction rings corresponding to two groups, one consisting of (200) and (112), and the other consisting of (100), (002), and (101), are too close to one other to be completely resolved. Figure 2(d) shows the bright field TEM image of ZnO nanoparticles annealed at 400 °C. It may be noted that randomly oriented nanoparticles with clear diffraction fringes are visible indicating crystalline quality of the annealed samples. The nanoparticles size was varying in the range of 6 to 9 nm and is shown in the inset of Figure 2(d). The nanoparticles were grown almost spherical or elliptical in shape which was advantageous for our experiments as the DEP force will be effective and nanoparticles assembly can be tuned accordingly.[12] An HRTEM image of a single ZnO nanoparticle shows the fringes corresponding to (002) plane with a lattice spacing (d) of about 0.259 nm. This d spacing is in agreement with the values estimated by XRD analysis and matches quite well with the literature reports.[35, 45, 46]

3.2. Dielectrophoretic Assembly of ZnO Nanoparticles

To assemble ZnO nanoparticles (~9 nm) into nanogap electrodes (60 nm), DEP process was used. DEP strongly depends on three parameters i.e., applied frequency (f), applied peak-to-peak voltage (V_{pp}), and trapping time (t) during which DEP is done. It is important to optimize the DEP parameters (f, V_{pp}, t) for consistent and reliable assembly of ZnO nanoparticles into nanogap electrodes. To investigate the effect of DEP parameters on the assembling of ZnO nanoparticles, experiments were carried out by varying one parameter and keeping the other two parameters fixed.

Figure 3 shows a schematic diagram of the setup used to perform DEP of ZnO nanoparticles into nanogap electrodes. Firstly, to optimize the effect of frequency variation on the nanoparticles assembling in nanogap electrodes, V_{pp} and t were maintained at 3 V and 60 s, respectively. Figures 4(a–c) show the SEM images of the assembly of nanoparticles at varying applied ac frequency (10, 150, and 600 kHz). It can be seen that assembling of nanoparticles strongly depends on the applied ac frequency. Applied frequency was varied from 10 kHz to 1 MHz, and it was interesting to observe that with an increase in frequency the assembly of ZnO nanoparticles into nanogap electrodes was steadily found to increase up to 150 kHz. However, the assembly was found to saturate beyond this frequency, and this behavior continued till 500 kHz. Interestingly, after 500 kHz, there was a gradual decrease in assembly of ZnO nanoparticles into nanogap electrodes, and very few

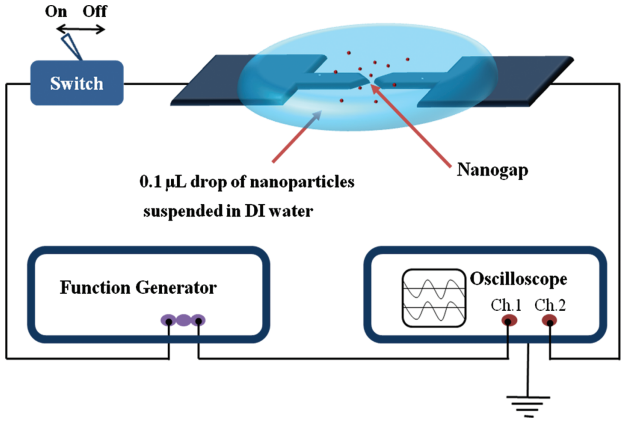

Fig. 3. Experimental setup consists of a pair of nanogap (60 nm) electrodes connected to a function generator and an oscilloscope. A period voltage signal is applied across the electrodes using a function generator to start the DEP process.

nanoparticles were seen in the vicinity of electrodes tip. A further increase in frequency to 1 MHz resulted in an interesting observation where electrodes were completely devoid of nanoparticles and latter were seen to repel from the region of high electric field strength to low electric field strength.[30]

During DEP process, the force acting on the particle known as DEP force (F_{DEP}) is expressed as[30, 47]:

$$F_{DEP} = 2\pi\varepsilon_0\varepsilon_m a^3 Re[K(\omega)]\Delta E_{rms} \quad (2)$$

where ε_m is the permittivity of the medium, a is the radius of the nanoparticle, $K(\omega)$ is the Clausius-Mosotti factor, and E_{rms} is the rms value of the electric field. The DEP force is proportional to $K(\omega)$, the volume of the nanoparticle and the gradient of the electric field. The frequency-dependent behavior resides in the Clausius-Mosotti factor, $K(\omega)$, and is given by[30]

$$K(w) = \frac{\varepsilon_p - \varepsilon_m - j/\omega(\sigma_p - \sigma_m)}{\varepsilon_p + 2\varepsilon_m - j/\omega(\sigma_p + 2\sigma_m)} \quad (3)$$

where ε_p and ε_m are the permittivities of the particle and medium, σ_p and σ_m are the conductivities of the particle and medium, j is $\sqrt{-1}$ and ω is $2\pi f$. This infers that the DEP force strongly depends on permittivities and conductivities of particle and medium, respectively. DEP force has two types, one is positive DEP and another is negative DEP. Positive DEP occurs when the $Re[K(\omega)]$ has positive value, and at that time a time-averaged force pulls the nanoparticles towards areas of strong electric field strength. The negative value of $Re[K(\omega)]$ causes negative DEP and corresponds to time-averaged force directing the nanoparticles towards areas of weak electric field strength. In the Clausius-Mosotti factor, the conductivity terms are dominant at low frequencies while the permittivity terms are dominant at high frequencies.[30] Following Eq. (3) and using the conductivities and permittivities of ZnO nanoparticles ($\varepsilon_p = 10\varepsilon_0$, $\sigma_p = 25$ μS/cm) and the medium (DI

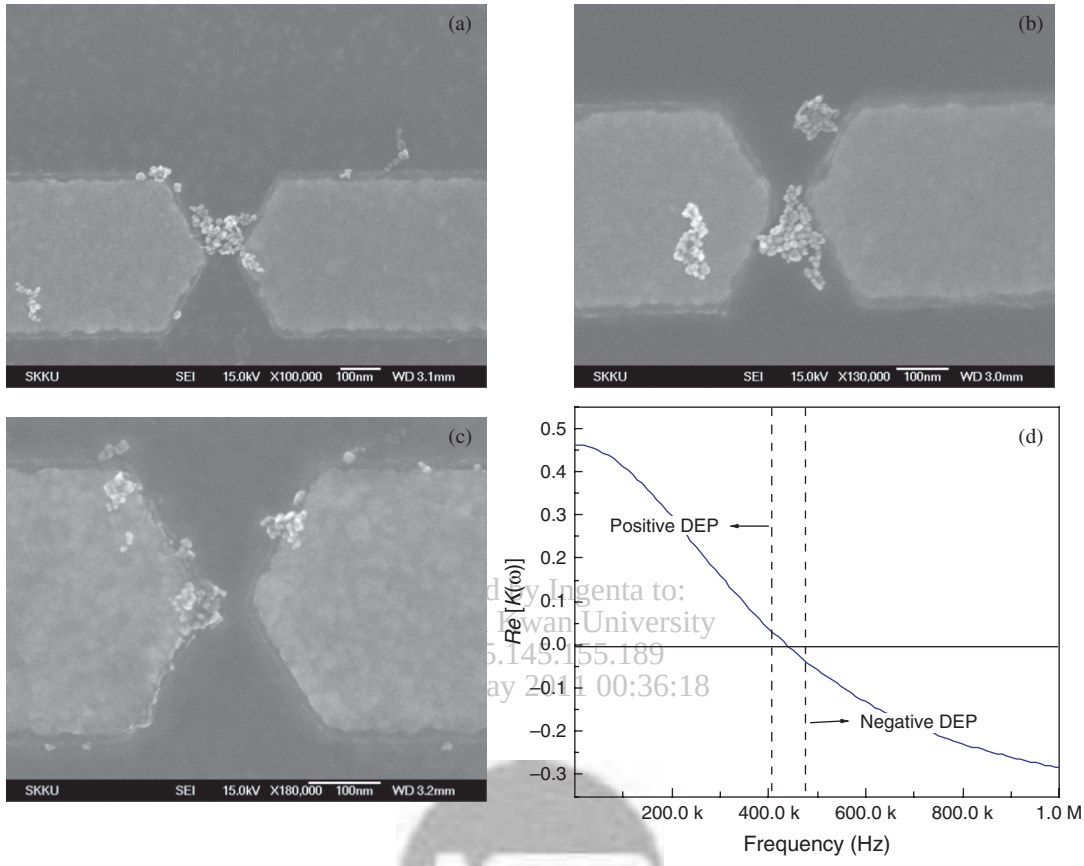

Fig. 4. (a–c) SEM images of the assembled ZnO nanoparticles into nanogap electrodes when the DEP was carried out at V_{pp} of 3 V, time of 30 s, and at different frequencies of 10, 150, and 600 kHz, respectively; (d) Graph shows the simulated result of variation in real parameter of Clausius-Mosotti factor, $Re[K(\omega)]$ with applied frequency (f). Positive DEP is dominant at frequencies below 500 kHz and negative DEP starts showing up its presence at frequencies close to 1 MHz.

water) ($\varepsilon_m = 80\varepsilon_0$, $\sigma_m = 7$ μS/cm), we simulated the real part of Clausius-Mosotti factor with applied frequency, and the result is shown as a graph in Figure 4(d), which is in agreement with the observations made in the present work (Figs. 4(a–c)). On comparing the observed behavior of DEP with the simulated curve, we conclude that at lower frequencies positive DEP force is dominant while at higher frequencies negative DEP is showing its presence and thus not allowing nanoparticles to remain in the regions of strong electric field. From the simulation curve the negative DEP is active at a frequency ≥450 kHz which is different than the experimentally observed values. Experimentally it was found that beyond frequency ≥600 kHz there was a gradual decrease in assembly of ZnO nanoparticles into nanogap electrodes, and a very few nanoparticles were seen in the vicinity of electrodes tip revealing the existence of negative DEP force. A little variation in results obtained experimentally and by theoretical simulation could be attributed to many factors which influence the DEP force, for examples, size-dependent permittivity and conductivity, electrode polarization, thermal effects, ac electroosmosis, etc.[12] With experimentation it was found that a frequency value of 150 kHz resulted in maximum yield of successful assembling, therefore, this frequency was chosen as the optimized DEP parameter for assembling maximum number of nanoparticles into nanogap electrodes. The number of nanoparticles into nanogap electrodes could further be controlled by varying the other two DEP parameters keeping frequency constant at 150 kHz.

To investigate the assembly under varying DEP time during which non-uniform electric field is active, f and V_{pp} were maintained at 150 kHz and 3 V, respectively. Figures 5(a–c) show the assembly of ZnO nanoparticles into nanogap electrodes under different assembly time of 30, 50, and 70 s, respectively. It may be noted that there was an increase in the assembly of nanoparticles when DEP was operated for a longer time. At a time of 30 s, a minimum number of nanoparticles were assembled in the nanogap electrodes. With increase in time the nanoparticles density was found to increase leading to large assembly in between the nanogap electrodes. For less than 30 s, the yield of assembly was too low, therefore, it was necessary to optmize the time to achieve the assembly of ZnO nanoparticles into nanogap electrodes. Figure 5(d) shows the variation of the average number of nanoparticles (including 5% error) assembled in the region between

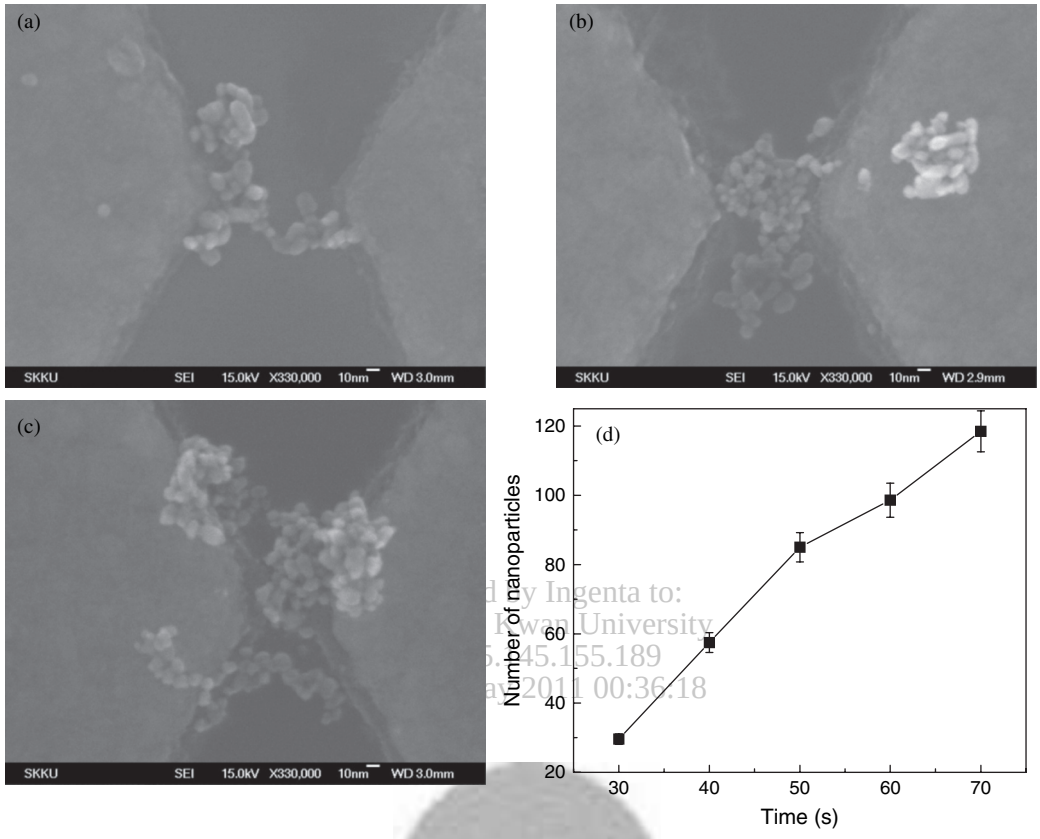

Fig. 5. (a–c) SEM images of the assembled ZnO nanoparticles into nanogap electrodes when the DEP was carried out at $f = 150$ kHz, $V_{pp} = 3$ V, and at different time of 30 s, 50 s, and 70 s, respectively; (d) Graph shows a variation of the average number of nanoparticles trapped in the nanogap electrodes with time.

the electrodes as a function of time. It is clearly seen that the number of assembled nanoparticles vary linearly with time. The DEP time was found to be an effective parameter to limit the number of nanoparticles assembly into nanogap electrodes.

To investigate the assembly under varying V_{pp}, the frequency of applied ac signal was kept at 150 kHz, and the DEP time was fixed at 30 s. Figures 6(a–c) show the SEM images of assembled ZnO nanoparticles under different V_{pp} of 2, 3, and 4 V, respectively. It can be inferred that as the applied voltage is increased, the number of nanoparticles assembled in the nanogap is also found to increase. It was found that V_{pp} had a maximum limit of 4 V with the present electrodes geometry because applied voltage beyond 4 V resulted in the burning of nanogap electrodes. Also, a higher voltage leads to electrolysis, and assembly rate is expected to reduce.

The mechanism of particle trapping in between the nanogap electrodes can be understood in the following way: The ZnO nanoparticles suspended in DI water remain under the action of electrophoretic effects before the application of alternating signal. These effects including Brownian motion lead to migration and subsequent deposition of nanoparticles between the regions of nanogap electrodes.[48] On application of a time varying electric field the migrational motions are suppressed due to induced polarization in these nanoparticles. The geometry of the electrodes gives rise to the field gradient in the regions between the electric field. If the dielectrophoretic force is strong enough to overcome the Brownian motion then the nature of electric field gradient decides the type of dielectrophoretic force on the nanoparticles. Such particle-field interaction strongly polarizes the particles and these particles retain strong dipole moment and tend to move in the region of strong electric field. The neighboring particles, due to particle–particle interactions, start chaining in the line of strongest electric field. Such particle-field and particle–particle interactions, no doubt reduce the DEP force, but help inducing particle chaining between the tips of the electrodes where electric field observes a maximum. Therefore, two effects play significant role in chaining and trapping of nanoparticles between nanogap electrodes, one is particle-field interaction and the other is particle–particle interaction. The chaining is observed when the combined effects overcome the Brownian motion. If we look at Eq. (2) then we understand that DEP force is strongly influenced by the strength of applied electric field. The type of DEP (positive or negative) is decided by real part of the $K(\omega)$, however, the strength of DEP force is directly proportional to the gradient of square of rms value

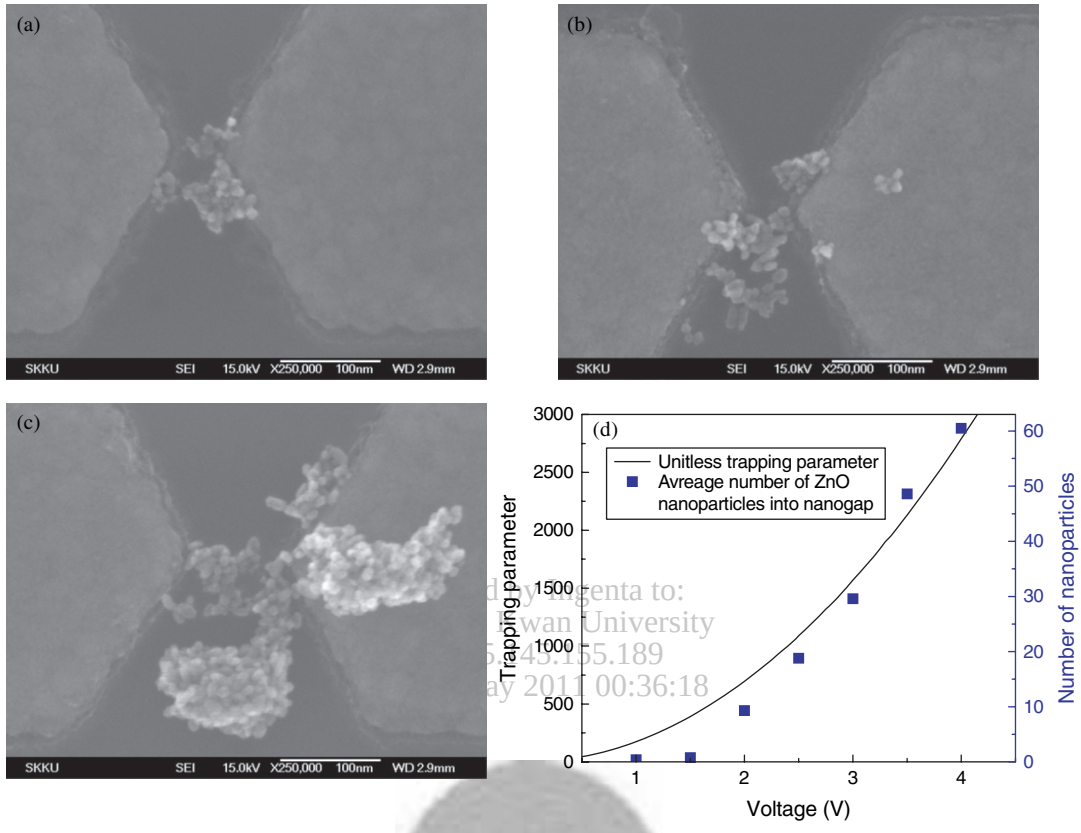

Fig. 6. (a–c) SEM images of the assembled ZnO nanoparticles into nanogap electrodes when the DEP was carried out at $f = 150$ kHz, $t = 30$ s, and at different V_{pp} of 2, 3, and 4 V, respectively. (d) Graph shows a variation of trapping parameter and the average number of trapped nanoparticles with applied voltage.

of electric field. To analyze the trapping and chaining formation of ZnO nanoparticles into nanogap electrodes, it is important to calculate the trapping parameter (η) for this system relative to ambient energy $k_B T$. The trapping parameter can be expressed as[48]

$$\eta = \frac{4\pi\varepsilon_0\varepsilon_m a^3 E_{rms}^2}{k_B T}\left(\frac{\varepsilon_p - \varepsilon_m}{\varepsilon_p + 2\varepsilon_m}\right) \quad (4)$$

where k_B is Boltzmann's constant, and T is the operating temperature. The trapping parameter was calculated using the Eq. (4) and plotted as a function of voltage applied between a pair of electrodes with a gap of 60 nm, as shown in Figure 6(d). In addition to trapping parameter, a plot corresponding to average number of nanoparticles with applied voltage is also shown for comparison. It may be noted that the average number of trapped ZnO nanoparticles in nanogap electrodes increases with increasing particle-field interactions i.e., trapping parameter. The trapping parameter calculated in the present work at an electric field strength of 5.0×10^7 V/m (applied voltage = 3 V) is ~1500 which is around 150 times larger than the values estimated by Ozturk et al.[48] for CdS nanoparticle clusters assembled in milli-meter sized electrodes gap under an applied field of $\sim 1.1 \times 10^5$ V/m (applied voltage = 110 V). The large value of trapping parameter suggests trapping is very effective in electrodes geometry used in the present work. It may further be noted that a trapping parameter of ~40 calculated for applied voltage of 0.5 V indicates that trapping is feasible in this system for all voltage values. However, we could not observe any assembly of nanoparticles below 2 V which shows that at these voltage values (<2 V) the DEP force is not strong enough to move the particles in the region of strong electric field and cause polarization. This suggests that DEP force should meet a critical value to overcome various forces in the system which influence the motion of the particle such as Brownian motion, gravity, and fluid flows induced by electric field, etc.[48–50] Moreover, the plot of average number of ZnO nanoparticles assembled in nanogap electrodes closely coincides with the curve of trapping parameter indicating a greater level of match in the experimental and theoretical results. The similar arguments explain the larger assembly of nanoparticles at longer DEP time. When DEP is performed for a longer time at a fixed applied voltage, the trapping parameter being significantly large (see Fig. 6(d)), the nanoparticles keep assembling in the electrodes gap until DEP process is stopped. This indicates that trapping parameter is directly proportional to DEP time.

3.3. Field Effect Characteristics of ZnO Based FET

The ZnO nanoparticles based device fabricated by DEP process was electrically characterized. The optimized DEP parameters i.e., $f = 150$ kHz, $V_{pp} = 3$ V, and $t = 30$ s have been used to assemble minimum number of ZnO nanoparticles into nanogap electrodes (60 nm). Such nano device is studied for FET characteristics. Figure 7(a) shows the schematic diagram of ZnO based FET assembled on p-type Si substrate capped with a 300 nm thick SiO_2 layer.

Figure 7(b) shows the typical current–voltage (I_D–V_{DS}) characteristic curves as a function of gate voltage (V_G) for the fabricated ZnO nanoparticles based FET. The curves indicate that the ZnO nanoparticles based FET exhibits a significant gate effect as the conductance of the ZnO nanoparticles increases with gate voltage suggesting n-type semiconducting behavior of ZnO nanoparticles. Figure 7(c) shows the I_d–V_G curves as a function of V_{DS} (0.5–2 V; step size: 0.5 V). The carrier mobility (μ) is calculated using the following relation[7, 9, 25]

$$\mu = g_m L^2 / C \cdot V_{DS} \quad (5)$$

where g_m is the transconductance defined as $\partial I_D / \partial V_G$ which is obtained from the linear region of the plot between I_D and V_G (Fig. 7(c)), L is the length of the nanoparticles assembly between the nanogap electrodes (60 nm), and C is the capacitance given by[7]

$$C = 2\pi\varepsilon\varepsilon_0 L / \ln(2h/r) \quad (6)$$

here, ε is the dielectric constant of silicon; h is thickness of silicon oxide layer (300 nm); and r is the radius of cylindrical channel consisting of ZnO nanoparticles (~50 nm; see Fig. 5(b)). The equations representing capacitance and mobility have been approximated for cylinders using an infinite plate model.[7] Using Eqs. (5) and (6), the electron mobility, μ was calculated to be ~29.7 cm^2/Vs which is in agreement with the previous reports on ZnO nanowires.[7, 9, 25]

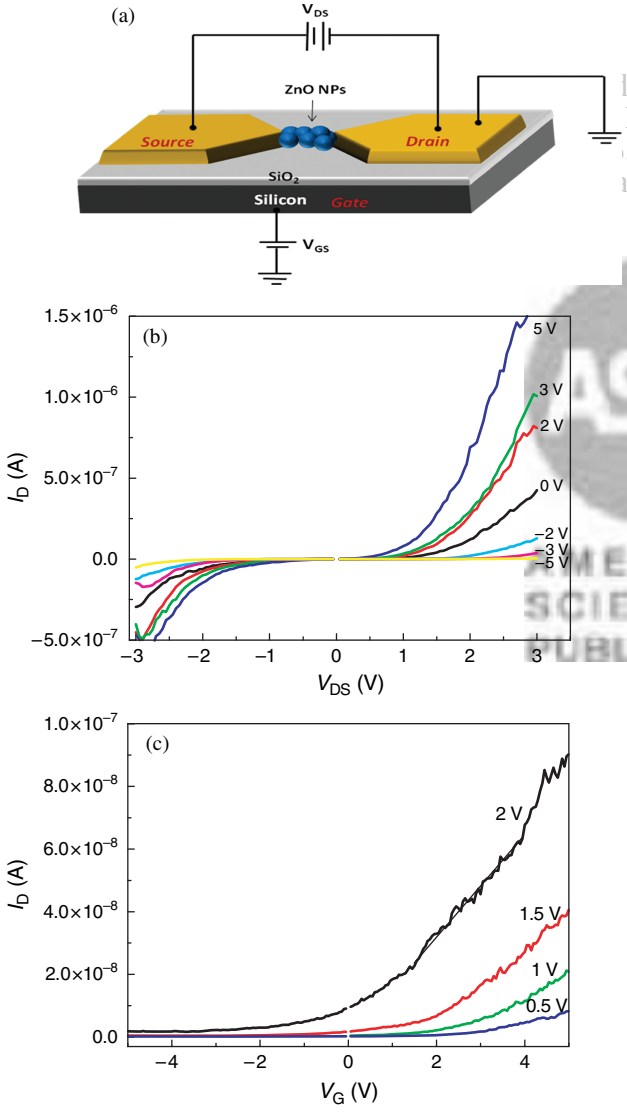

Fig. 7. (a) Schematic diagram of ZnO nanoparticles based FET assembled on SiO_2/Si substrate; (b) Typical I_D–V_{DS} characteristics curves as a function of V_G showing a typical n-type semiconducting behavior of ZnO nanoparticles; (c) I_D–V_G curves of dielectrophoretically fabricated ZnO nanoparticles FET operating in a n-channel mode as a function of V_{DS}.

4. CONCLUSIONS

ZnO nanoparticles of diameter ranging from 6 to 9 nm have been grown by sol–gel method. Analytical techniques showed that grown material after annealing exhibited good crystalline quality. These nanoparticles have been assembled into nanogap electrodes under various DEP experimental conditions. Frequency variation study revealed the observation of positive and negative DEP forces; whereas the trapping parameter was found to vary with applied voltage. Optimization of various DEP parameters such as frequency of 150 kHz, peak-to-peak voltage of 3 V, and time of 30 s led to the assembly of few nanoparticles in the nanogap electrodes. ZnO based nanodevice exhibited field effect characteristics when configured in the form of an FET. Results reveal the potential of ZnO nanoscale devices for applications in electronic and optoelectronic.

Acknowledgment: This research was supported by WCU (World Class University) Program through the National Research Foundation of Korea (NRF) funded by the Ministry of Education, Science and Technology (R32-2008-000-10204-0).

References and Notes

1. K. Mølhave, T. M. Hansen, D. N. Madsen, and P. Bøggild, *J. Nanosci. Nanotechnol.* 4, 279 (**2004**).
2. L. Liao, H. B. Lu, J. C. Li, C. Liu, D. J. Fu, and Y. L. Liu, *Appl. Phys. Lett.* 91, 173110 (**2007**).

RESEARCH ARTICLE

3. S. S. Hullavarad, N. V. Hullavarad, P. C. Karulkar, A. Luykx, and P. Valdivia, *Nanoscale Res. Lett.* 2, 161 (**2007**).
4. Q. Wan, Q. H. Li, Y. J. Chen, T. H. Wang, X. L. He, J. P. Li, and C. L. Lin, *Appl. Phys. Lett.* 84, 3654 (**2004**).
5. Q. H. Li, Q. Wan, Y. X. Liang, and T. H. Wang, *Appl. Phys. Lett.* 84, 4556 (**2004**).
6. M. S. Arnold, P. Avouris, Z. W. Pan, and Z. L. Wang, *J. Phys. Chem. B* 107, 659 (**2003**).
7. W. I. Park, J. S. Kim, G. C. Yi, M. H. Bae, and H. J. Lee, *Appl. Phys. Lett.* 85, 5052 (**2004**).
8. C. Soci, A. Zhang, B. Xiang, S. A. Dayeh, D. P. R. Aplin, J. Park, X. Y. Bao, Y. H. Lo, and D. Wang, *Nano Lett.* 7, 1003 (**2007**).
9. Z. Fan, D. Wang, P. C. Chang, W. Y. Tseng, and J. G. Lu, *Appl. Phys. Lett.* 85, 5923 (**2004**).
10. Z. Fan and J. G. Lu, *Appl. Phys. Lett.* 86, 123510 (**2005**).
11. J. W. Lee, K. J. Moon, M. H. Ham, and J. M. Myoung, *Solid State Commun.* 148, 194 (**2008**).
12. B. C. Gierhart, D. G. Howitt, S. J. Chen, R. L. Smith, and S. D. Collins, *Langmuir* 23, 12450 (**2007**).
13. S. H. Yoon, S. Kumar, G.-H. Kim, Y. S. Choi, T. W. Kim, and S. I. Khondaker, *J. Nanosci. Nanotechnol.* 8, 3427 (**2008**).
14. P. R. C. Gascoyne and J. Vykoukal, *Electrophoresis* 23, 1973 (**2002**).
15. Z. Chen, Z. Y. Wu, L. M. Tong, H. P. Pan, and Z. F. Liu, *Anal. Chem.* 78, 8069 (**2006**).
16. C. Zhang, K. Khoshmanesh, A. Mitchell, and K. Kalantar-Zadeh, *Anal. Bioanal. Chem.* 396, 401 (**2010**).
17. Y. B. Li, Y. Bando, T. Sato, and K. Kurashima, *Appl. Phys. Lett.* 81, 144 (**2002**).
18. S. Kumar, G.-H. Kim, K. Sreenivas, and R. P. Tandon, *J. Phys.: Condens. Matter.* 19, 472202 (**2007**).
19. A. B. Hartanto, X. Ning, Y. Nakata, and T. Okada, *Appl. Phys. A* 78, 299 (**2004**).
20. J. J. Wu, S. C. Liu, C. T. Wu, K. H. Chen, and L. C. Chen, *Appl. Phys. Lett.* 81, 1312 (**2002**).
21. H. Yan, B. Messer, M. Law, and P. Yang, *Adv. Mater.* 14, 158 (**2007**).
22. D. Park and K. Yong, *J. Vac. Sci. Technol. B* 26, 1933 (**2008**).
23. J. Carrey, H. Carrére, M. L. Kahn, B. Chaudret, X. Marie, and M. Respaud, *Semicond. Sci. Technol.* 23, 025003 (**2008**).
24. J. Suehiro, N. Nakagawa, S. Hidaka, M. Ueda, K. Imasaka, M. Higashihata, T. Okada, and M. Hara, *Nanotechnology* 17, 2567 (**2006**).
25. S. K. Lee, S. Y. Lee, J. H. Hyung, C. O. Jang, D. J. Kim, and D. I. Suh, *J. Nanosci. Nanotechnol.* 8, 3473 (**2008**).
26. C. S. Lao, J. Liu, P. Gao, L. Zhang, D. Davidovic, R. Tummala, and Z. L. Wang, *Nano Lett.* 6, 263 (**2006**).
27. G. Cheng, Z. Li, S. Wang, H. Gong, K. Cheng, X. Jiang, S. Zhou, Z. Du, T. Cui, and G. Zou, *Appl. Phys. Lett.* 93, 123103 (**2008**).
28. O. Harnack, C. Pacholski, H. Weller, A. Yasuda, and J. M. Wessels, *Nano Lett.* 3, 1097 (**2003**).
29. E. A. Meulenkamp, *J. Phys. Chem. B* 102, 5566 (**1998**).
30. S. Kumar, Y.-G. Seo, and G.-H. Kim, *Appl. Phys. Lett.* 94, 153104 (**2009**).
31. J. Zhou, F. Zhao, Y. Wang, Y. Zhang, and L. Yang, *J. Luminescence* 122–123, 195 (**2007**).
32. H. Wang and C. Xie, *J. Phy. Chem. Sol.* 69, 2440 (**2008**).
33. V. Noack and A. Eychmüller, *Chem. Mater.* 14, 1411 (**2002**).
34. H. Kleinwechter, C. Janzen, J. Knipping, H. Wiggers, and P. Roth, *J. Mater. Sci.* 37, 4349 (**2002**).
35. P. K. Giri, S. Bhattacharyya, D. K. Singh, R. Kesavamoorthy, B. K. Panigrahi, and K. G. M. Nair, *J. Appl. Phys.* 102, 093515 (**2007**).
36. P. Hoyer, R. Eichberger, and H. Weller, *Ber. Bunsen-Ges. Phys. Chem.* 97, 630 (**1993**).
37. L. E. Brus, *J. Chem. Phys.* 80, 4403 (**1984**).
38. W. Q. Peng, S. C. Qu, G. W. Cong, and Z. G. Wang, *Mater. Sci. Semicond. Proc.* 9, 156 (**2006**).
39. T. S. Tan, B. J. Chen, X. W. Sun, W. J. Fan, H. S. Kwok, X. H. Zhang, and S. J. Chua, *J. Appl. Phys.* 98, 013505 (**2005**).
40. V. Ischenko, S. Polarz, D. Grote, V. Stavarache, K. Fink, and M. Driess, *Adv. Funct. Mater.* 15, 1945 (**2005**).
41. U. Koch, A. Fojtik, H. Weller, and A. Henglein, *Chem. Phys. Lett.* 122, 507 (**1985**).
42. V. Noack and A. Eychmüller, *Chem. Mater.* 14, 1411 (**2002**).
43. E. Burstein, *Phys. Rev.* 93, 632 (**1954**).
44. T. S. Moss, *Proc. Phys. Soc., London B* 67, 775 (**1954**).
45. F. Rataboul, C. Nayral, M. J. Casanove, A. Maisonnat, and B. Chaudret, *J. Organ. Chem.* 643, 307 (**2002**).
46. H. Zhang, D. Yang, Y. Ji, X. Ma, J. Xu, and D. Que, *J. Phys. Chem. B* 108, 3955 (**2004**).
47. R. J. Barsotti, M. D. Vahey, R. Wartena, Y. M. Chiang, J. Voldman, and F. Stellacci, *Small* 3, 488 (**2007**).
48. B. Ozturk, I. Talukdar, and B. N. Flanders, *Appl. Phys. Lett.* 86, 183105 (**2005**).
49. M. Li, Y. Qu, Z. Dong, Y. Wang, and W. J. Li, *IEEE Trans. Nanotechnol.* 7, 477 (**2008**).
50. H. W. Seo, C. S. Han, D. G. Choi, K. S. Kim, and Y. H. Lee, *Microelectron. Eng.* 81, 83 (**2005**).

Received: 16 February 2010. Accepted: 28 July 2010.

RESEARCH ARTICLE